Optics Letters

Particle tracking by repetitive phase-shift interferometric super resolution microscopy

Itay Gdor,[1] Xiaolei Wang,[1] Matthew Daddysman,[1] Yuval Yifat,[1] Rosemarie Wilton,[2] Mark Hereld,[3] Marie-Françoise Noirot-Gros,[2] and Norbert F. Scherer[1,*]

[1]James Franck Institute, University of Chicago, 5801 S Ellis Ave, Chicago, Illinois 60637, USA
[2]Biosciences Division, Argonne National Laboratory, 9700 S. Cass Avenue, Lemont, Illinois 60439, USA
[3]Mathematics and Computer Science Division, Argonne National Laboratory, 9700 S. Cass Avenue, Lemont, Illinois 60439, USA
*Corresponding author: nfschere@uchicago.edu

Received 28 March 2018; revised 12 May 2018; accepted 13 May 2018; posted 15 May 2018 (Doc. ID 326382); published 7 June 2018

Accurate and rapid particle tracking is essential for addressing many research problems in single molecule and cellular biophysics and colloidal soft condensed matter physics. We developed a novel three-dimensional interferometric fluorescent particle tracking approach that does not require any sample scanning. By periodically shifting the interferometer phase, the information stored in the interference pattern of the emitted light allows localizing particles positions with nanometer resolution. This tracking protocol was demonstrated by measuring a known trajectory of a fluorescent bead with sub-5 nm axial localization error at 5 Hz. The interferometric microscopy was used to track the RecA protein in *Bacillus subtilis* bacteria to demonstrate its compatibility with biological systems.

OCIS codes: (180.0180) Microscopy; (110.2650) Fringe analysis; (120.4640) Optical instruments; (120.5060) Phase modulation; (170.2520) Fluorescence microscopy; (120.3180) Interferometry.

https://doi.org/10.1364/OL.43.002819

Optical microscopy is one of the most common and useful tools to study biological systems. Optical imaging is facile, rapid, and (relatively) nondestructive, which allows *in vivo* measurements of living cells and organisms [1]. The ability to track and monitor individual particle movement in real time is one of the most crucial tools to gain information and shed light on a variety of open biological questions [2,3]. There are, however, two main limitations in pursuing ideal three-dimensional (3D) tracking: one is the modest optical resolution that limits the ability to localize the particle in space; and the other is accessing axial information by scanning the sample in the Z-axis direction, which degrades the time resolution.

The spatial resolution of a conventional optical microscope is fundamentally limited by the wavelength and the numerical aperture (NA) of the objective lens [4]. While shorter wavelengths improve the resolution, the approach is limited by the transparency of the optical elements and the biological materials themselves. Additionally, short wavelength illumination increases phototoxicity in live samples [5]. As for improving the NA, the light collecting angle is close to its practical maximum in modern commercially available objectives, so little room is left for further improvement. Other approaches such as computational deconvolution [6,7], multiphoton microscopy [3,8], and confocal [1] and light sheet microscopy [9,10] have improved the lateral resolution and to lesser degree the axial resolution.

Nevertheless, axial resolution remains unsatisfactory because a conventional lens only collects a hemispherical wavefront propagating from the sample toward the lens and cannot collect angles on the "back side" of the sample. If an imaging system could produce a complete spherical wavefront, the focal point, due to symmetry, would be (nearly) spherical, resulting in axial resolution that is similar to its lateral counterpart [11]. Expanding the detection to collect emission in both axial directions is equivalent to increasing the aperture angle of the system [12]. In addition, light collection in opposing directions and with two detectors doubles the number of photons collected, but also implementing interferometry would make it the dominant determinant of the axial resolution.

Beyond improvement of the aperture angle, when the optical path lengths of the two axial imaging paths of the microscope are within the coherence length, the two beams of light interfere with each other at the detector. Since the phase of the resulting interference pattern is highly sensitive to the position of the emitter, high resolution information in the axial direction is embedded in the interference fringes. Illuminating from both sides increases the contrast by creating an interference pattern in the illumination as well. Encoding high frequency spatial information in the interference fringes is the key principle for widefield I^2M/I^5M [13] and in spot-scanning 4Pi microscopy [14], providing up to sevenfold improvement in axial resolution [15]. Shtengel *et al.* [16] recorded three phase-shift images in an interferometric microscope using a three-way beamsplitter allowing single-shot measurement of a particle's 3D position with sub-20-nm localization. Recently, Wang *et al.* [17] used small modifications of the path length of one of the arms in an interferometric microscope to scan over different phases, achieving 2 nm localization at 1 Hz.

To avoid the need for Z scanning, Ram *et al.* [18] developed multifocal microscopy recording more than one plane at a time. The use of a diffractive-optic element [19] allows capturing an entire 3D focal stack that can be recorded in a single exposure of the camera (at the expense of the XY field of view). Abrahamsson *et al.* [20] successfully used this method for tracking RNA polymerase II at the optical diffraction limit. Fourier-based structured illumination sensing [21] as well as double-helix [22] and tetrapod [23] engineered point spread functions (PSFs) localize particles beyond the diffraction limit but may be overwhelmed by overlapping particles in dense samples.

Welsher and Yang [24] demonstrated sub-10-nm tracking resolution in three dimensions by actively keeping the sample in the same position using active feedback and a 3D piezo nanopositioner. While the results are impressive, this approach can only track a single particle at a time.

In this paper we show how the two main limitations, the need to scan along the Z plane and the microscope's axial resolving power, can be overcome using an interferometric microscope.

Our setup, shown in Fig. 1(a), is an in-house built I^2M/I^5M microscope based on the design reported by Gustafsson *et al.* [13]. For I^5M, the illuminating incoherent light-emitting diode (LED) light (Thorlabs; M490L4) was split into two equal intensity beams by a beamsplitter. Each beam is sent to one of two opposing objective lenses (Olympus; UPLSAPO60X) and focused to the same focal plane where the fluorescent sample is mounted. The sample-emitted fluorescence is collected by the same opposing objectives to form magnified images that are combined by the same beamsplitter. The result of the two outputs of the interferometer are imaged and recorded by two electron-multiplying CCD (EM-CCD) cameras (Andor; iXon 888). In the I^2M configuration the illuminating incoherent LED light is sent through only one of the objectives, but the collection is the same as in the I^5M. After loading the sample, a waiting period (~1 h) is required in order for the microscope to achieve passive stability. At that time the microscope maintains 20 nm (20 nm = 0.2 rad) phase stability for 1 h of measurement time, which is adequate since each data set takes only 1–3 min to acquire.

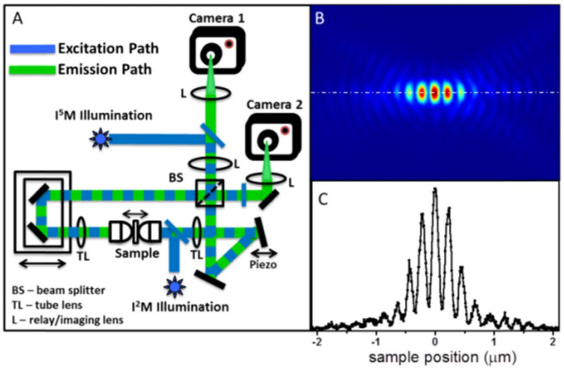

Fig. 1. Experimental setup and PSF for our interferometric (I^2M/I^5M) microscope. (a) Scheme of I^2M/I^5M setups. The sample emission (green line) is collected using both objectives and interferes at the detectors. The optical path lengths are controlled by a pair of mirrors on a translator stage (Newport; XMS100) and the phase modulation is done by a mirror on a piezo stage (Mad-city lab; Nano-OP100). (b) PSF: YZ view of a 100-nm diameter fluorescent bead measured in I^2M mode. (c) Z cut through the PSF presented in (b).

Figure 1(b) shows the YZ plane of the PSF of the I^2M microscope measured by scanning a 100 nm diameter fluorescent bead along the axial direction with 10 nm steps. A Z-cut through the center of the PSF image [white dashed line in Fig. 1(b)] is shown in Fig. 1(c). The I^2M PSF exhibits a clear interference pattern that contains the high resolution information.

High position localization information is extracted from the intensity modulations of the optical interference, which depends on the position of the particle between the two objectives. Wang *et al.* [17] used this strong dependence in order to study *E. coli* RNA by continuously scanning the phase of the standing wave, thus effectively scanning the sample without moving it.

We found that this localization problem can be simplified further. In practice, achieving interferometric resolution in the axial axis only requires two phase measurements with $\pi/2$ shift between them. Mathematically the interference is sinusoidal; thus particle localization within one wavelength simply involves calculating the phase. However, because sine is not an injective function, measuring the amplitude at one position of the sample is not enough to uniquely establish the particle location. Rather, measuring the interference intensity at two phases with $\pi/2$ shift between them, namely, measuring $\sin(\varphi)$ and $\sin(90+\varphi)$ [equivalent to measuring $\sin(\varphi)$ and $\cos(\varphi)$], is sufficient. Dividing the two measurements results in a tangent function, which is injective, from which φ can be readily extracted. In order to record two measurements with the desired shift between them, we changed the path length of one of the arms in the microscope with a $\pi/2$ shift of the standing wave and performed this repetitively in a square wave fashion throughout the measurement.

To demonstrate the method, the integrated intensity emitted from a fluorescent bead adhered to a glass coverslip was measured as a function of the bead position while moving the bead axially between the objectives. The data, separated into the two phases [$\sin(\varphi)$ and $\sin(90+\varphi)$ functions], is presented in Fig. 2(a). Due to intensity variation along the microscope focus that can be seen in the gradually changing shape in Fig. 2(a), background noise, and readout offset, we found that using a single camera is not sufficient to accurately determine φ. This issue can be solved by adding a second camera and measuring the second output of the beamsplitter [see Fig. 1(a)]. At first glance, the second camera does not add any additional information as a π shift is inherent between both cameras; if camera 1 measures $\sin(\varphi)$, camera 2 will measure $\sin(\pi+\varphi) = -\sin(\varphi)$, as demonstrated in Fig. 2(b). Nevertheless, subtraction of the second camera output doubles the amplitude (doubles the number of photons detected) and eliminates the undesired offset, giving a signal that is symmetric around zero [see Fig. 2(c)]. The latter increases the accuracy of position determination by reducing the number of variables required to describe the function. Figure 2(c) demonstrates the intensity of both phases as a function of bead position; the ratio between those two phases is displayed in Fig. 2(d). The resulting phase as extracted by applying the arctangent function on this ratio is shown in Fig. 2(e).

Since the phase is expected to change linearly with the position of the particle, we could use this to determine the accuracy and error of particle tracking. Figure 3 is a calibration

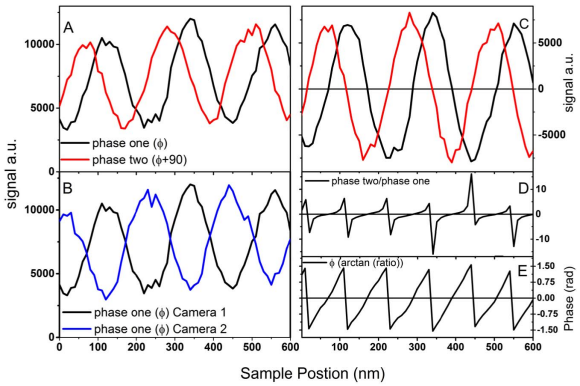

Fig. 2. Fluorescence signal and phase reconstruction from our repetitive phase shifting I^{2}M. (a) Intensity of the emitted light as a function of bead position for two phases of the interferometer. (b) Intensity of emitted light as a function of bead position as recorded with two cameras for a single position of the phase changing mirror. (c) Emitted light intensity extracted following subtraction of the simultaneously recorded images of the two cameras, for two phases as a function of bead position. (d) Ratio between the two phases presented in panel (c). (e) Measured particle phase as a function of the bead position extracted using the arctan function.

curve to extract the relation between the phase and the sample position. From the slope we determined that translation of 109 ± 1 nm is equal a full π shift, as expected from the emission wavelength in water ($n = 1.3$) and the PSF interference pattern in Fig. 1.

The relation between the measured phase and the true position determined from the calibration curve was then used to track a fluorescent bead that was moved by a piezo translator in a triangular waveform over 0.5 μm in the axial direction. We applied the aforementioned algorithm to extract the bead's axial position. The result is compared with the true value given by the piezo translator's internal encoder as shown in Fig. 4(a). The results demonstrate that the system can track the motion of the beads with standard error of 4 nm in the localization measured at 5 Hz. To demonstrate 3D tracking, the orientation of the translator that held the sample was slightly altered so the movement along the Z axis was accompanied by small movements along the X and Y axes. The resulting XY tracking is presented in Fig. 4(b). The localization in the XY plane was achieved by 2D Gaussian fitting to find the particle position in

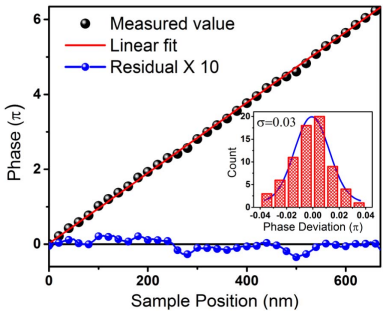

Fig. 3. Calibration curve giving the relation between the phase and the position based on the data presented in Fig. 2. The fit gives an error of ±1 nm corresponding to our localization error. The distribution of the residuals is shown in the inset.

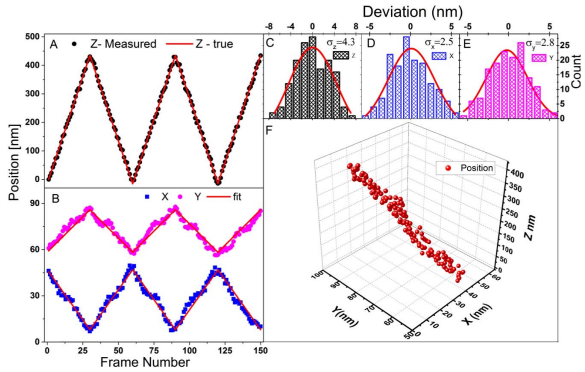

Fig. 4. Results of interferometric particle tracking at 5 Hz. (a) Fluorescent bead moved in a triangle form Z trajectory (black points) compared with the true position (red line) obtained from the piezo translator encoder. (b) XY trajectory of the same bead, extracted using a 2D Gaussian fit. (c), (d), and (e) are the distribution of the residuals for Z, X, and Y, respectively, along with Gaussian fit. (f) 3D trajectory of the fluorescent bead.

every frame [25]. As the true position of the particle in XY is unknown but linearly proportional to the known Z position, the error in the equatorial plane was estimated under the assumption that the periodic motion of the fluorescent bead repeats its path identically and any deviation in the value measured is a result of localization error. Under this assumption the standard error is measured from the deviation from a linear fit. The distributions of the individual axes' residuals are shown in Figs. 4(c), 4(d), and 4(e) along with Gaussian fits. The final 3D trajectory of the bead is presented in Fig. 4(f). 3D localization of a single fluorescent bead immobilized on a coverslip at an acquisition rate of 5 Hz is presented in Visualization 1.

In order to demonstrate the ability to track and record the trajectory of several particles simultaneously, we measured a sample containing 100 nm diameter fluorescent beads in 80% glycerol solution. Figure 5(a) presents six 2D trajectories (XY) superimposed on the first frame recorded (the full movie is presented in Visualization 2 in the Supporting Information). Two of those trajectories are presented in 3D in Figs. 5(b) and 5(c). The bead's diffusion constant at 20°C was calculated to be $0.045 \cdot 10^{-6}$ cm^2/s versus the expected value of $0.035 \cdot 10^{-6}$ cm^2/s.

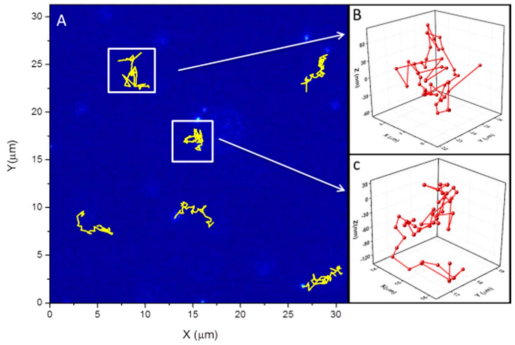

Fig. 5. 2D and 3D trajectories of 100 nm fluorescent beads in glycerol solution, measured at 5 Hz. (a) Six 2D trajectories (XY) superimposed on the raw image. (b) and (c) Two trajectories presented in 3D. The trajectories chosen are marked with white squares.

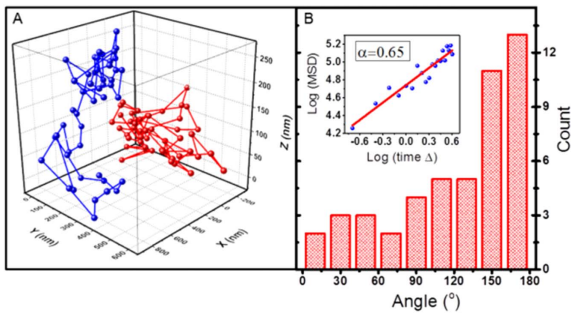

Fig. 6. Tracking RecA–GFP protein. (a) 3D trajectory of two RecA–GFP complexes (in two cells) during spore development. (b) Directionality of adjacent steps of RecA protein reversals hindered motion; Inset: MSD calculation for the trajectory.

We demonstrate the interferometric tracking method on a biological system by imaging and tracking the fluorescence from a RecA–green fluorescent protein (GFP) fusion in *Bacillus subtilis*. RecA protein has an essential role in the repair and maintenance of bacterial DNA [26] by promoting homologous DNA strand exchange through formation of a dynamic nucleoprotein filament [27]. During spore formation, RecA also forms transient and mobile foci associated to the nucleoid of the mother cell during spore development [28]. The RecA–GFP fusion protein complex constitutes a single spot in each bacterium. Figure 6 presents a 3D trajectory of two RecA–GFP complexes (in two cells) during spore development. These two trajectories were determined using the method described previously from measurements presented in Supporting Information Visualization 3. Contrary to the fluorescent bead, the results reveal that the movement of RecA is not Brownian in nature, covering a large percentage of the available cell volume in less than 5 s. In addition, the mean square displacement (MSD) reveals a clear subdiffusive dynamic ($\alpha = 0.65$), a value similar to the one previously measured for m-RNA in bacteria [29].

We presented a new method for super resolution 3D particle tracking without the need for sample scanning based on repetitive phase shifting in an interferometric microscope. The ability to localize a particle to within 4 nm in all dimensions was demonstrated as well as concurrent 3D localization of multiple particles over a large field of view and the capability to track moving fluorescent proteins in live bacteria. Therefore interferometric microscopy combined with a new data analysis algorithm enables fast and reliable particle tracking with superior resolution.

While the interferometric periodic modulation method presented here provides a fast and powerful option for super resolution 3D particle tracking, it still has one experimental challenge that needs to be addressed. As the interference is a periodic function, the algorithm always assumes that the particle movement was the shortest distance required to reach the new phase. For example, if the particle moves by $3/2\pi$ between measurements, the algorithm will assume that it moved by $-\pi/2$. Thus, the system cannot accurately measure positions of particles that move further than half the wavelength between measurements. As the main limitation regarding frame rate is the need to change the path length of one of the arms between measurements (the piezo translator, carrying the 2" dia. turning mirror, requires ~0.1 s to reach and stabilize at the new position), we are currently working on a "solid state" approach that will have the ability to record all four phases in a single shot.

Funding. U.S. Department of Energy (DOE) (DE-AC02-06CH11357).

Acknowledgment. We thank Professors Oliver Cossairt and Aggelos Katsaggelos for helpful discussions and Prof. John Sedat for technical advice. This work was supported by the Biological Systems Science Division, Office of Biological and Environmental Research, Office of Science, U.S. Department of Energy.

REFERENCES

1. J. B. Pawley, *Handbook of Biological Confocal Microscopy* (2006).
2. M. J. Saxton and K. Jacobson, Annu. Rev. Biophys. Biomol. Struct. **26**, 373 (1997).
3. V. Levi, Q. Q. Ruan, and E. Gratton, Biophys. J. **88**, 2919 (2005).
4. M. Born and E. Wolf, *Principles of Optics: Electromagnetic Theory of Propagation, Interference and Diffraction of Light* (1994).
5. J. N. Post, K. A. Lidke, B. Rieger, and D. J. Arndt-Jovin, FEBS Lett. **579**, 325 (2005).
6. P. Campisi and K. Egiazarian, *Blind Image Deconvolution: Theory and Applications* (CRC Press, 2016).
7. P. Sarder and A. Nehorai, IEEE Signal Process. Mag. **23**, 32 (2006).
8. W. R. Zipfel, R. M. Williams, and W. W. Webb, Nat. Biotechnol. **21**, 1369 (2003).
9. J. Huisken, J. Swoger, F. Del Bene, J. Wittbrodt, E. H. K. Stelzer, J. Huisken, J. Swoger, F. Del Bene, J. Wittbrodt, and E. H. K. Stelzer, Science **1007**, 13 (2014).
10. P. A. Santi, J. Histochem. Cytochem. **59**, 129 (2011).
11. S. Hell and E. H. K. Stelzer, Opt. Commun. **93**, 277 (1992).
12. S. Hell, Science **2316**, 1153 (2007).
13. M. G. L. Gustafsson, D. A. Agard, J. W. Sedat, and S. Francisco, J. Microsc. **195**, 10 (1999).
14. M. Nagorni and S. W. Hell, J. Struct. Biol. **123**, 236 (1998).
15. M. G. Gustafsson, Curr. Opin. Struct. Biol. **9**, 627 (1999).
16. G. Shtengel, J. A. Galbraith, C. G. Galbraith, J. Lippincott-Schwartz, J. M. Gillette, S. Manley, R. Sougrat, C. M. Waterman, P. Kanchanawong, M. W. Davidson, R. D. Fetter, and H. F. Hess, Proc. Natl. Acad. Sci. USA **106**, 3125 (2009).
17. G. Wang, J. Hauver, Z. Thomas, S. A. Darst, and A. Pertsinidis, Cell. **167**, 1839 (2016).
18. S. Ram, P. Prabhat, J. Chao, E. S. Ward, and R. J. Ober, Biophys. J. **95**, 6025 (2008).
19. L. Sacconi, E. Froner, R. Antolini, M. R. Taghizadeh, A. Choudhury, and F. S. Pavone, Opt. Lett. **28**, 1918 (2003).
20. S. Abrahamsson, J. Chen, B. Hajj, S. Stallinga, A. Y. Katsov, J. Wisniewski, G. Mizuguchi, P. Soule, F. Mueller, C. D. Darzacq, X. Darzacq, C. Wu, C. I. Bargmann, D. A. Agard, M. Dahan, and M. G. L. Gustafsson, Nat. Methods **10**, 60 (2013).
21. D. Feldkhun and K. H. Wagner, Opt. Lett. **41**, 3483 (2016).
22. S. R. P. Pavani, M. A. Thompson, J. S. Biteen, S. J. Lord, N. Liu, R. J. Twieg, R. Piestun, and W. E. Moerner, Proc. Natl. Acad. Sci. USA **106**, 2995 (2009).
23. Y. Shechtman, L. E. Weiss, A. S. Backer, S. J. Sahl, and W. E. Moerner, Nano Lett. **15**, 4194 (2015).
24. K. Welsher and H. Yang, Nat. Nanotechnol. **9**, 198 (2014).
25. R. E. Thompson, D. R. Larson, and W. W. Webb, Biophys. J. **82**, 2775 (2002).
26. B. S. Zhou and S. J. Elledge, Nature **408**, 433 (2000).
27. A. Kuzminov, Proc. Natl. Acad. Sci. USA **98**, 8461 (2001).
28. V. Bidnenko, L. Shi, A. Kobir, M. Ventroux, N. Pigeonneau, C. Henry, A. Trubuil, M. F. Noirot-Gros, and I. Mijakovic, Mol. Microbiol. **88**, 921 (2013).
29. I. Golding and E. C. Cox, Phys. Rev. Lett. **96**, 098102 (2006).